

DESY 96-213
hep-ph/9612203
November 1996

Deep Inelastic Scattering with Tagged Photons at HERA

D. Bardin ^{a,b}, L. Kalinovskaya ^{b,1}, and T. Riemann ^a

^a Deutsches Elektronensynchrotron DESY, Institut für Hochenergiephysik, Platanenallee 6, D-15738 Zeuthen, Germany

^b Bogoliubov Laboratory for Theoretical Physics, Joint Institute for Nuclear Research, ul. Joliot-Curie 6, RU-141980 Dubna, Russia

Abstract

We calculate cross-sections for neutral current deep inelastic scattering at HERA with photon tagging. Both, the exact lowest-order cross-section and a leading logarithmic approximation of next-order corrections are calculated. The latter amounts to less than 20% in a large kinematical range. The integrations are performed numerically but without relying on Monte Carlo methods.

¹Supported by the Heisenberg-Landau Program

1 Introduction

We calculate cross-section predictions for the reaction

$$e(k_1) + p(p_1) \longrightarrow e(k_2) + X(p_2) + \gamma(k), \quad (1.1)$$

where the photon is assumed to be observed (tagged). The calculated cross-section will be differential in energy E'_e and angle θ'_e of the final state electron and in the energy E_γ^{vis} of the photon. Equivalently, the usual scaling variables x, y together with E_γ^{vis} may be chosen². The angular range covered by the photon tagging device is taken into account by kinematical cuts in the course of integrations. In the numerical results we will follow the experimental set-up of the H1 collaboration with the photon tagging device located in the forward direction with respect to the electron beam³. The lowest-order cross-section is determined without approximations. Since one expects large photonic corrections in some kinematical ranges, we tried to estimate them with a leading logarithmic approximation. What we do is certainly not a rigorous approach and cannot replace a complete second-order calculation. In this connection the neglect of effects due to photon interferences has to be mentioned. They are of next-to-leading order, but may be non-negligible for a forward tagging device. For the time being, we hope to cover the most substantial corrections.

In Section 2, the lowest-order cross-section is calculated, Section 3 contains a discussion of the inclusive cross-section. The leading-logarithmic corrections are calculated in Section 4 and numerical results are presented in Section 5. Some technical details may be found in the Appendix.

2 The Lowest-Order Cross-Section

In this section we derive a set of formulae, which allow the lowest-order description of deep-inelastic cross-sections with tagged photons, where the latter may have arbitrary kinematics. Obviously, the treatment of arbitrary cuts in energy and production angles is possible only with numerical methods. Thus, we decided to tackle the problem not with the semi-analytical approach as developed in our previous papers. Instead, we will numerically integrate the squared matrix element over the phase space imposing the appropriate cuts explicitly. For this aim, we use natural variables in the HERA system. Besides the four-momenta of initial state electron and proton, this are variables, which are directly measured by the apparatus: angles and energies of final state electron, E'_e, θ'_e , and of the photon, $E_\gamma, \theta_\gamma, \varphi_\gamma$. The following representations for the 4-vectors p_1, k_1, k_2, k have been chosen (see also Figure 1):

$$p_1 = (E_p, 0, 0, -p_p), \quad (2.1)$$

$$k_1 = (E_e, 0, 0, p_e), \quad (2.2)$$

² We note that the usual definition of x and y in terms of leptonic variables is used. They are not recalculated using the reduced electron beam energy after emission of the observed photon.

³ This direction is called backward direction [with respect to the proton beam] in the H1 collaboration.

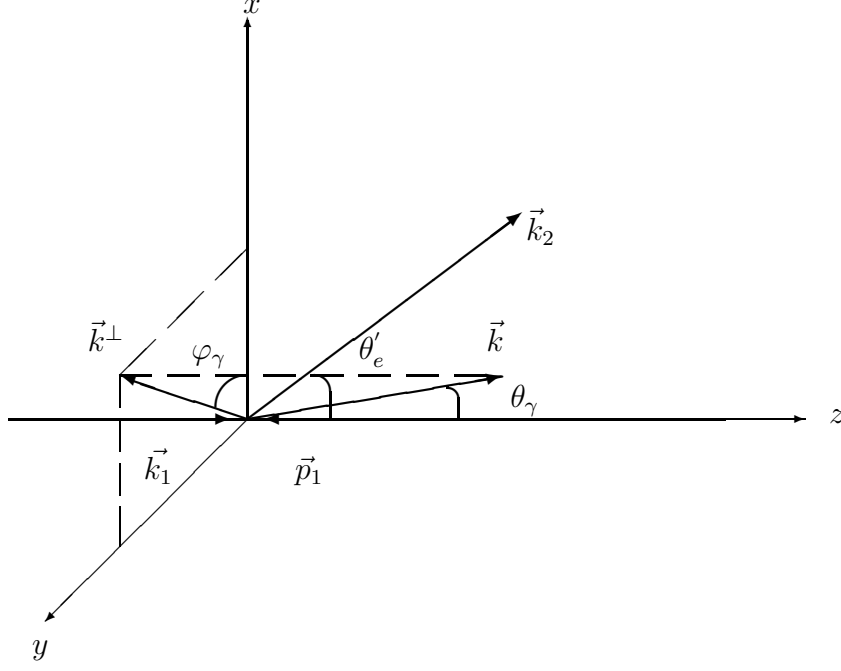


Figure 1: *Three-momenta in the HERA frame*

$$k_2 = (E'_e, p'_e \sin \theta'_e, 0, p'_e \cos \theta'_e), \quad (2.3)$$

$$k = E_\gamma(1, \sin \theta_\gamma \cos \varphi_\gamma, \sin \theta_\gamma \sin \varphi_\gamma, \cos \theta_\gamma), \quad (2.4)$$

$$p_2 = p_1 + k_1 - k_2 - k. \quad (2.5)$$

In these variables, the invariants s, Q_l^2, y_l are:

$$s = (k_1 + p_1)^2 = (E_e + E_p)^2 - (p_e - p_p)^2 = S + M^2 + m^2, \quad (2.6)$$

$$S = 2p_1 k_1 = 2(E_e E_p + p_e p_p), \quad (2.7)$$

$$y_l = \frac{p_1(k_1 - k_2)}{p_1 k_1} = 1 - 2(E_p E'_e + p_p p'_e \cos \theta'_e)/S, \quad (2.8)$$

$$Q_l^2 = -(k_1 - k_2)^2 = 2(E_e E'_e - p_e p'_e \cos \theta'_e) - 2m^2. \quad (2.9)$$

With m and M we denote the electron and proton masses, respectively. We will also use the π production threshold,

$$\bar{M} = M + m_\pi, \quad (2.10)$$

which is the lowest mass of the inelastic final hadronic system.

The angular variables are unlimited,

$$-1 \leq \cos \theta'_e \leq +1, \quad (2.11)$$

$$-1 \leq \cos \theta_\gamma \leq +1, \quad (2.12)$$

$$0 \leq \varphi_\gamma \leq 2\pi, \quad (2.13)$$

while the allowed ranges of electron and photon energies have to be determined:

$$m \leq E'_e \leq E'_e{}^{\max}(\theta'_e), \quad (2.14)$$

$$0 \leq E_\gamma \leq E_\gamma{}^{\max}(E'_e, \theta'_e, \theta_\gamma, \varphi_\gamma). \quad (2.15)$$

The upper limits are derived in Appendix A:

$$E'_e{}^{\max} = \frac{1}{S_\theta} \left[(E_e + E_p)(E_e E_p + p_e p_p + m^2 - \Delta M^2/2) + (p_e - p_p) \cos \theta'_e \sqrt{L_\theta} \right], \quad (2.16)$$

with

$$L_\theta = (E_e E_p + p_e p_p + m^2 - \frac{1}{2} \Delta M^2)^2 - m^2 S_\theta, \quad (2.17)$$

$$S_\theta = (E_e + E_p)^2 - (p_e - p_p)^2 \cos^2 \theta'_e, \quad (2.18)$$

$$\Delta M^2 = \bar{M}^2 - M^2, \quad (2.19)$$

and

$$E_\gamma{}^{\max} = \frac{S + 2m^2 + M^2 - \bar{M}^2 - 2(E_e + E_p)E'_e + 2(p_e - p_p)p'_e \cos \theta'_e}{2[E_e + E_p - E'_e + (p'_e \cos \theta'_e - [p_e - p_p]) \cos \theta_\gamma + p'_e \sin \theta'_e \sin \theta_\gamma \cos \varphi_\gamma]}. \quad (2.20)$$

The phase space is defined as follows:

$$d\Gamma = \frac{d\vec{k}_2}{2k_2^0} \frac{d\vec{k}}{2k^0} \frac{d\vec{p}_2}{2p_2^0} dM_h^2 \delta^4(k_1 + p_1 - k_2 - k - p_2), \quad (2.21)$$

with

$$M_h^2 = (p_1 + k_1 - k_2 - k)^2. \quad (2.22)$$

We show in appendix A that the doubly-differential phase space in terms of natural variables takes the following form:

$$\frac{d\Gamma}{p'_e dE'_e d\cos \theta'_e} = \frac{\pi}{2} \int_0^{2\pi} d\varphi_\gamma \int_{-1}^{+1} d\cos \theta_\gamma \int_0^{E_\gamma{}^{\max}} E_\gamma dE_\gamma. \quad (2.23)$$

The totally differential cross-section in natural variables is:

$$\frac{d^5 \sigma_{\text{brem}}}{d\cos \theta'_e dE'_e d\cos \theta_\gamma d\varphi_\gamma dE_\gamma} = \frac{4\alpha^3}{\pi S} p'_e E_\gamma \frac{1}{Q_h^4} \sum_{i=1}^3 S_i \mathcal{F}_i. \quad (2.24)$$

The functions \mathcal{F}_i are generalized structure functions. Explicit expressions for them may be found in Equations (I.2.18) ⁴.

⁴ Here and henceforth, we mark equations taken from reference [1] with I.

The totally differential ‘radiator functions’ S_i for the radiative process are, with account of minor improvements and modifications, taken from Equations (I.2.40)–(I.2.42):

$$S_1 = -2m^2 Q_h^2 \left(\frac{1}{z_1^2} + \frac{1}{z_2^2} \right) + \frac{Q_l^4 + Q_h^4}{z_1 z_2} + 2, \quad (2.25)$$

$$S_2 = \frac{1}{S y_h} \left\{ -2m^2 \left[\frac{S^2 y_{l_1} (y_{l_1} + y_h) - M^2 Q_h^2}{z_1^2} + \frac{S^2 (1 - y_h) - M^2 Q_h^2}{z_2^2} \right] + \frac{S^2 Q_h^2 (Y_+ - y_l y_h) - M^2 (Q_l^4 + Q_h^4)}{z_1 z_2} - S^2 y_h \left(\frac{1}{z_1} + \frac{y_{l_1}}{z_2} \right) - 2M^2 \right\}, \quad (2.26)$$

$$S_3 = \frac{1}{y_h} \left\{ -m^2 Q_h^2 \left[\frac{2y_{l_1} + y_h}{z_1^2} + \frac{2 - y_h}{z_2^2} \right] + \frac{Q_l^2 Q_h^2 (2 - y_l)}{z_1 z_2} - Q_h^2 \left(\frac{y_{l_1}}{z_1} - \frac{1}{z_2} \right) - y_h \frac{Q_l^2 + Q_h^2}{2} \left(\frac{1}{z_1} + \frac{1}{z_2} \right) \right\}. \quad (2.27)$$

Above, we retained m where needed and M throughout. The following abbreviations and definitions have been used:

$$y_{l_1} = 1 - y_l, \quad (2.28)$$

$$Y_+ = 1 + y_{l_1}^2, \quad (2.29)$$

$$y_h = \frac{p_1(p_2 - p_1)}{p_1 k_1} = y_l - \frac{2E_\gamma}{S} (E_p + p_p \cos \theta_\gamma), \quad (2.30)$$

$$z_1 = 2k_1 k = 2E_\gamma (E_e - p_e \cos \theta_\gamma), \quad (2.31)$$

$$\begin{aligned} z_2 &= 2k_2 k = z_1 + Q_l^2 - Q_h^2 \\ &= 2E_\gamma \left[E'_e - p'_e \left(\cos \theta'_e \cos \theta_\gamma + \sin \theta'_e \sin \theta_\gamma \cos \varphi_\gamma \right) \right], \end{aligned} \quad (2.32)$$

$$\begin{aligned} Q_h^2 &= -(p_2 - p_1)^2 \\ &= Q_l^2 - 2E_\gamma \left[(p_e - p'_e \cos \theta'_e) \cos \theta_\gamma - p'_e \sin \theta'_e \sin \theta_\gamma \cos \varphi_\gamma + E'_e - E_e \right]. \end{aligned} \quad (2.33)$$

The definitions reflect the radiative kinematics: the difference $Q_h^2 - Q_l^2$ as well as z_1 and z_2 are proportional to E_γ . In Appendix A, the same is shown for $W^2 - M_h^2$.

From the above expressions, any radiative cross-section, if measured in natural variables, may be calculated by simply imposing the corresponding cuts when integrating (2.24).

The lowest-order radiative cross-section becomes:

$$\frac{d^3 \sigma_{\text{brem}}}{d \cos \theta'_e dE'_e dE_\gamma} = \frac{4\alpha^3}{\pi S} p'_e \int d \cos \theta_\gamma \int d \varphi_\gamma \frac{E_\gamma}{Q_h^4} \sum_{i=1}^3 S_i \mathcal{F}_i, \quad (2.34)$$

with reasonably defined boundaries for the angular integrations. In case of a forward tagging device as being used by the H1 and ZEUS collaborations:

$$\cos \theta_\gamma \in \left(1 - \frac{1}{2}\Delta\theta_\gamma^2, 1\right), \quad \varphi_\gamma \in (0, 2\pi). \quad (2.35)$$

Here, $\Delta\theta_\gamma$ describes the opening angle of the tagging device⁵.

For applications, it may be useful finally to change variables:

$$\frac{d^3\sigma_{\text{brem}}}{dx_l dy_l dE_\gamma} = \mathcal{J} \frac{d^3\sigma_{\text{brem}}}{d\cos\theta'_e dE'_e dE_\gamma}, \quad (2.36)$$

with $Q_l^2 = x_l y_l S$. The Jacobean is easily determined from (2.8) and (2.9):

$$\mathcal{J} = \left| \frac{\partial(\cos\theta'_e, E'_e)}{\partial(x_l, y_l)} \right| = \frac{y_l S}{2p'_e}. \quad (2.37)$$

We show the lowest-order cross-sections (2.36) in Figures 2 and 3 for $E_\gamma = 5, 10$ GeV and $\Delta\theta_\gamma = 0.5$ mrad. The updated Fortran program HECTOR [2] with flag settings ISSE=1 and ISCH=0 (selecting structure functions CTEQ3(L0)) is used for all numerical results. As is seen in the figures, the minimal value of y depends on both x and $E_\gamma^{\text{vis}} = E_\gamma$. In addition, it depends on the angular cuts. For a forward tagging device, its absolute minimum may be approximated by

$$y_c = \frac{E_\gamma^{\text{vis}}}{E_e}. \quad (2.38)$$

The cross-section resembles the typical behavior of inclusive deep inelastic scattering.

3 The Inclusive Cross-Section

In the preceding Section, we made the assumption that the energy of the tagged photon will be observed. Events with vanishing photon energy were automatically excluded and thus all the problems related to the infrared singularity. In this Section, we will treat the photon energy as inclusive variable, i.e. determine the doubly-differential cross-section $d^2\sigma/d\cos\theta'_e dE'_e$ as the sum of Born cross-section, vertex correction, and real bremsstrahlung contributions:

$$\frac{d^2\sigma}{d\cos\theta'_e dE'_e} = \frac{d^2\sigma_{\text{Born}}}{d\cos\theta'_e dE'_e} (1 + \delta_{\text{vert}}) + \int dE_\gamma \frac{d^3\sigma_{\text{brem}}}{dE_\gamma d\cos\theta'_e dE'_e}. \quad (3.1)$$

The purpose is two-fold. We want to have the opportunity to perform a numerical comparison of the present, deterministic calculations with those performed in the semi-analytical approach; and the latter are doubly-differential. Further, in the next Section we estimate

⁵ Strictly speaking, one should take into account the actual form of the tagger (being e.g. rectangular rather than circular); we leave this as an exercise to the reader.

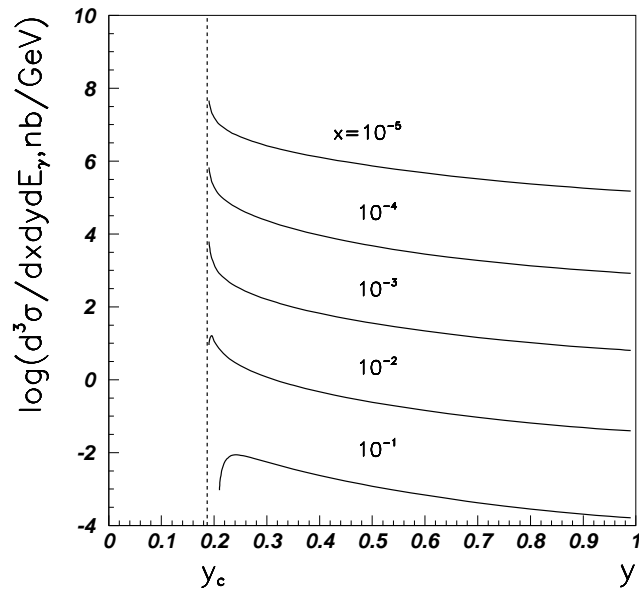


Figure 2: *Lowest-order cross-section for HERA kinematics with $E_\gamma = 5 \text{ GeV}$ and $\Delta\theta_\gamma = 0.5 \text{ mrad}$*

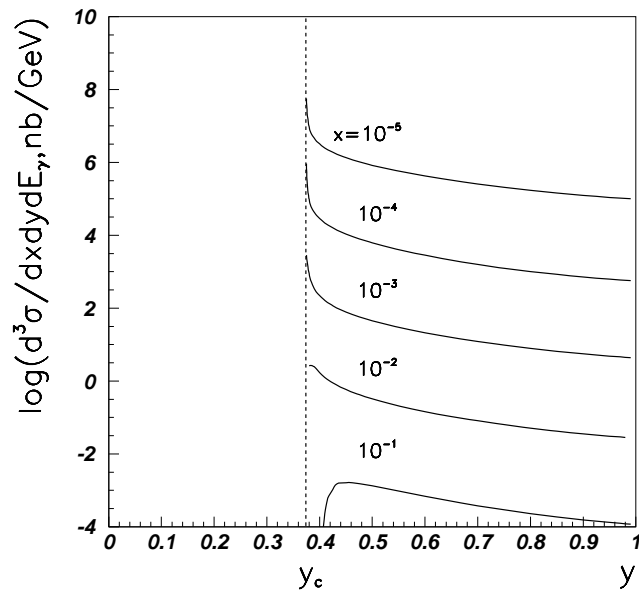


Figure 3: *The same as Figure 2 but with $E_\gamma = 10 \text{ GeV}$*

higher-order QED corrections using the leading-logarithmic approximation for them. In doing so, we will have to make use of (2.34) without a restriction on the lower limit of E_γ .

We will consider (2.34) without cuts on the photonic angles,

$$\frac{d^3\sigma_{\text{brem}}}{d\cos\theta'_e dE'_e dE_\gamma} = \frac{4\alpha^3}{\pi S} p'_e \int_{-1}^1 d\cos\theta_\gamma \int_0^{2\pi} d\varphi_\gamma \frac{E_\gamma}{Q_h^4} \sum_{i=1}^3 S_i \mathcal{F}_i, \quad (3.2)$$

and derive the lowest-order QED corrections $d^2\sigma_{\text{QED}}/dx_l dy_l$ to the cross-section

$$\frac{d^2\sigma_{\text{theor}}}{dx_l dy_l} = \frac{d^2\sigma_{\text{Born}}}{dx_l dy_l} + \frac{d^2\sigma_{\text{QED}}}{dx_l dy_l}. \quad (3.3)$$

Then, $d^2\sigma_{\text{QED}}$ has to be compared to the semi-analytical result, see e.g. Equations (I.4.40) and (I.5.3). For this aim, we have to multiply (3.2) by the Jacobean (A.8), then to integrate over E_γ , and therefore to regularize the infrared divergence. From (3.1), the $d^2\sigma_{\text{QED}}$ is to be calculated now:

$$\begin{aligned} \frac{d^2\sigma_{\text{QED}}}{d\cos\theta'_e dE'_e} &= \int_{-1}^{+1} d\cos\theta_\gamma \int_0^{2\pi} d\varphi_\gamma \int_0^{E_\gamma^{\text{max}}} dE_\gamma \left\{ \frac{d^5\sigma_{\text{brem}}}{d\cos\theta'_e dE'_e d\cos\theta_\gamma d\varphi_\gamma dE_\gamma} \theta(E_\gamma - \bar{E}_\gamma) \right. \\ &\quad \left. + \frac{1}{\Delta\Omega_\gamma} \frac{d^2\sigma_{\text{Born}}}{d\cos\theta'_e dE'_e} [1 + \delta_{\text{VR}}(\bar{E}_\gamma)] \delta(E_\gamma) \right\}, \end{aligned} \quad (3.4)$$

with a cutoff \bar{E}_γ on the minimum photon energy for the numerical integration. The correction δ_{VR} will be discussed below. Further, it is

$$\Delta\Omega_\gamma = \int d\cos\theta_\gamma \int d\varphi_\gamma. \quad (3.5)$$

In (3.4), the angular integrations are unrestricted, $\Delta\Omega_\gamma = 4\pi$ and $d^5\sigma_{\text{brem}}$ is a completely differential, infrared-finite bremsstrahlung cross-section and may be treated numerically as it stands. It is the analogue to Equation (I.5.3) without the subtracted terms.

In fact, we have to follow a different strategy for the solution of the soft-photon problem. In the semi-analytical approach, we performed a subtraction of the infrared divergent part of the integrand thus making the numerical integration infrared finite in the limit $E_\gamma \rightarrow 0$. This subtraction was compensated by an analytical integration of the subtracted part. We specially had to choose a reference frame where the limits of photon energy variation are independent of the angular variables, this way considerably simplifying the integrations. This was possible since the net cross-section was defined in a covariant way. Here, the situation is quite different. We have to use the above defined set of natural variables in order to finally be allowed to apply the cuts. As was discussed, the photon energy varies in limits which depend in a complicated way on the photon angles. It is important for the calculation that one may choose \bar{E}_γ so small that it is well inside a region where E_γ is *unrestricted* by the photon angles. That this region exists for arbitrary values of θ'_e, E'_e may be seen in Figure 9 where the allowed region for photon energies is shown below the shaded surface as function of these angles. At $\cos\theta_\gamma = 0$, the minimal

E_γ^{\max} is reached. If \bar{E}_γ is smaller, there is no influence of the photon angles on the photon energy boundary. We have to choose:

$$\bar{E}_\gamma < \frac{S + 2m^2 + M^2 - \bar{M}^2 - 2(E_e + E_p)E'_e + 2(p_e - p_p)p'_e \cos \theta'_e}{2[E_e + E_p - E'_e + (p'_e \cos \theta'_e - [p_e - p_p])]} \quad (3.6)$$

We split the correction into pieces as it was done in (I.4.40):

$$\begin{aligned} \frac{d^2 \sigma_{\text{QED}}}{d \cos \theta'_e dE'_e} &= \frac{\alpha}{\pi} \delta_{\text{vert}} \frac{d^2 \sigma_{\text{Born}}}{d \cos \theta'_e dE'_e} + \frac{d^2 \sigma_{\text{soft}}^{\text{IR}}}{d \cos \theta'_e dE'_e} + \frac{d^2 \sigma_{\text{hard}}^{\text{IR}}}{d \cos \theta'_e dE'_e} + \frac{d^2 \sigma_{\text{R}}^{\text{F}}}{d \cos \theta'_e dE'_e} \\ &\equiv \frac{\alpha}{\pi} \delta_{\text{VR}}(\bar{E}_\gamma) \frac{d^2 \sigma_{\text{Born}}}{d \cos \theta'_e dE'_e} + \frac{d^2 \sigma_{\text{R}}^{\text{F}}}{d \cos \theta'_e dE'_e}, \end{aligned} \quad (3.7)$$

with

$$\delta_{\text{VR}}(\bar{E}_\gamma) = \delta_{\text{vert}}(\mu) + \delta_{\text{soft}}^{\text{IR}}(\epsilon, \mu) + \delta_{\text{hard}}^{\text{IR}}(\epsilon, \bar{E}_\gamma). \quad (3.8)$$

Here, $d^2 \sigma_{\text{R}}^{\text{F}}/d \cos \theta'_e dE'_e$ is the result of the numerical integration of the first term in (3.4) and the Born cross-section is:

$$\frac{d^2 \sigma_{\text{Born}}}{d \cos \theta'_e dE'_e} = \frac{4\pi\alpha^2 p'_e}{S Q_l^4} \sum_{i=1}^3 S_i^{\text{B}} \mathcal{F}_i, \quad (3.9)$$

with the Born radiators

$$S_1^{\text{B}} = 2Q_l^2, \quad (3.10)$$

$$S_2^{\text{B}} = \frac{2}{S y_l} \left[(1 - y_l) S^2 - M^2 Q_l^2 \right], \quad (3.11)$$

$$S_3^{\text{B}} = \frac{2 - y_l}{y_l} Q_l^2. \quad (3.12)$$

The hard part of the infrared divergent corrections is defined by Equation (I.4.8):

$$\delta_{\text{hard}}^{\text{IR}}(\epsilon, \bar{E}_\gamma) = \frac{1}{\pi} \int_{\epsilon}^{\bar{E}_\gamma} dE_\gamma E_\gamma \int_{-1}^1 d \cos \theta_\gamma \int_0^{2\pi} d\varphi_\gamma \mathcal{F}^{\text{IR}} = 2 \ln \frac{\bar{E}_\gamma}{\epsilon} \left(\ln \frac{Q_l^2}{m^2} - 1 \right), \quad (3.13)$$

where \mathcal{F}^{IR} is the Low factor (see e.g. Equation (I.4.5)):

$$\mathcal{F}^{\text{IR}} = \frac{Q^2}{z_1 z_2} - m^2 \left(\frac{1}{z_1^2} + \frac{1}{z_2^2} \right). \quad (3.14)$$

The integrals used are given in the Appendix.

The infrared divergent part of the soft photon contribution is:

$$\delta_{\text{soft}}^{\text{IR}}(\epsilon, \mu) = \frac{1}{\pi} \int_0^\epsilon dE_\gamma E_\gamma \int_{-1}^1 d \cos \theta_\gamma \int_0^{2\pi} d\varphi_\gamma \mathcal{F}^{\text{IR}}. \quad (3.15)$$

With its calculation, one may follow Reference I until reaching Equation (I.4.26):

$$\delta_{\text{soft}}^{\text{IR}}(\epsilon, \mu) = 2 \left[\mathcal{P}^{\text{IR}} + \ln \frac{2\epsilon}{\mu} \right] \left[(Q_l^2 + 2m^2)L_m - 1 \right] + \mathcal{S}_\Phi + \frac{1}{2\beta_1} \ln \frac{1+\beta_1}{1-\beta_1} + \frac{1}{2\beta_2} \ln \frac{1+\beta_2}{1-\beta_2}, \quad (3.16)$$

with

$$L_m = \frac{1}{\sqrt{\lambda_m}} \ln \frac{\sqrt{\lambda_m} + Q_l^2}{\sqrt{\lambda_m} - Q_l^2}, \quad (3.17)$$

$$\lambda_m = Q_l^2(Q_l^2 + 4m^2). \quad (3.18)$$

Calculating (3.16) in the ultrarelativistic limit, with β_1 and β_2 being the velocities of the initial and final state electrons in the HERA frame, the infrared divergent part gets:

$$\delta_{\text{soft}}^{\text{IR}}(\epsilon, \mu) = 2 \left(P^{\text{IR}} + \ln \frac{2\epsilon}{\mu} \right) \left(\ln \frac{Q_l^2}{m^2} - 1 \right) + \ln \frac{4E_e E'_e}{m^2} + \mathcal{S}_\Phi. \quad (3.19)$$

The function \mathcal{S}_Φ also reflects the dependence of the soft photon treatment on the reference system in which the corrections $\delta_{\text{soft}}^{\text{IR}}$ and $\delta_{\text{hard}}^{\text{IR}}$ are calculated. We calculate \mathcal{S}_Φ numerically using the integral representation:

$$\mathcal{S}_\Phi = \frac{1}{2} (Q^2 + 2m^2) \int_0^1 \frac{d\alpha}{\beta_\alpha k_\alpha^2} \ln \frac{1-\beta_\alpha}{1+\beta_\alpha}, \quad (3.20)$$

with

$$k_\alpha = k_1 \alpha + k_2 (1 - \alpha), \quad (3.21)$$

$$\beta_\alpha = \frac{|\vec{k}_\alpha|}{k_\alpha^0}, \quad (3.22)$$

$$k_\alpha^2 = Q_l^2 \alpha (1 - \alpha) + m^2, \quad (3.23)$$

$$|\vec{k}_\alpha|^2 = p_e^2 \alpha^2 + (p'_e)^2 (1 - \alpha)^2 + 2p_e p'_e \cos \theta'_e \alpha (1 - \alpha), \quad (3.24)$$

$$k_\alpha^0 = E_e \alpha + E'_e (1 - \alpha). \quad (3.25)$$

The infrared singularity is compensated by the contribution from the QED vertex correction (see e.g. Equation (I.4.34)):

$$\delta_{\text{vert}}(\mu) = -2 \left(P^{\text{IR}} + \ln \frac{m}{\mu} \right) \left(\ln \frac{Q_l^2}{m^2} - 1 \right) - \frac{1}{2} \ln^2 \frac{Q_l^2}{m^2} + \frac{3}{2} \ln \frac{Q_l^2}{m^2} - 2 + \frac{\pi^2}{6}. \quad (3.26)$$

In sum:

$$\delta_{\text{VR}}(\bar{E}_\gamma) = 2 \ln \frac{2\bar{E}_\gamma}{m} \left(\ln \frac{Q_l^2}{m^2} - 1 \right) - \frac{1}{2} \ln^2 \frac{Q_l^2}{m^2} + \frac{3}{2} \ln \frac{Q_l^2}{m^2} + \ln \frac{4E_e E'_e}{m^2} - 2 + \frac{\pi^2}{6} + \mathcal{S}_\Phi. \quad (3.27)$$

In practice, we took $\bar{E}_\gamma = 10^{-4}$ GeV and verified stability against variations. With the Fortran program HECTOR, we further confirmed numerically with high precision that cross-section (3.7) agrees with that calculated in the semi-analytical approach provided no cut is applied.

4 Higher-Order Initial-State Radiation in Leading-Logarithmic Approximation

So far we considered the lowest-order cross-section. A calculation of higher-order photonic contributions is a non-trivial task since the cross-section is not completely inclusive. We will apply the leading-logarithmic approximation (LLA) which worked amazingly well for inclusive cross-sections (see, e.g., [1]).

We begin with the generic LLA formula for photonic initial state corrections,

$$\frac{d^2\sigma^{\text{ini}}}{d\cos\theta'_e dE'_e} = \int_0^1 dz \rho(z) \left\{ \frac{d^2\sigma_{\text{QED}}}{d\cos\theta'_e dE'_e} \Big|_{E_e \rightarrow zE_e} \Theta_z - \frac{d^2\sigma_{\text{QED}}}{d\cos\theta'_e dE'_e} \right\}. \quad (4.1)$$

The totally inclusive $\mathcal{O}(\alpha)$ density is:

$$\rho(z) = \frac{\alpha}{2\pi} \frac{1+z^2}{1-z} \left(\ln \frac{Q_f^2}{m^2} - 1 \right). \quad (4.2)$$

Only the initial electron energy scales,

$$E_e \rightarrow \hat{E}_e = zE_e. \quad (4.3)$$

The kinematical limits (2.16) and (2.20) of the final state energies depend on the actual values of the angles and on \hat{E}_e, E_p . Thus, we have to introduce a step function,

$$\Theta_z = \Theta(\hat{W}^2 - M^2) \Theta(\hat{M}_h^2 - M^2), \quad (4.4)$$

in order to ensure the non-trivial kinematical conditions (A.1) and (A.2). Further, we note that the Jacobean is unity in (4.1) since this differential cross-section is being calculated in terms of variables which do not scale with $E_e \rightarrow zE_e$.

How is the cross-section (4.1) related to an experiment with photon tagging? Formally, one has to ‘differentiate’ (4.1) with respect to the visible photon energy. But we have to care about the definition of E_γ^{vis} . And this depends largely on the specific experimental set-up. There are two different cases to be considered:

- Case (i)
The tagging device is *not in forward direction* of the electron beam;
- Case (ii)
It *is in forward direction* of the electron beam.

The relevant object to be calculated is the three-fold differential cross-section

$$\frac{d^3\sigma}{d \cos \theta'_e dE'_e dE_\gamma^{\text{vis}}}, \quad (4.5)$$

where the visible photon energy is the energy deposited in the tagging device.

We see two potential sources of inaccuracy which could make our calculations less reliable than usual applications of LLA often are:

- For tagging in non-forward direction, the assumption of inclusiveness of the process in the LLA photon angle is fulfilled approximately while tagging in forward direction has to be treated with care (see below).
- The photon, which is treated with the LLA method and that of the Born cross-section are identical particles but they are treated differently and their interferences are neglected. The treatment assumes them to be distinguishable. The resulting inaccuracy, though, is of next-to-leading order.

4.1 Case (i): Non-Forward Tagging Device

In Case (i), the visible photon energy is simply

$$E_\gamma^{\text{vis},(i)} = E_\gamma. \quad (4.6)$$

The LLA describes the emission of collinear photons, here from the initial electron. These forward photons cannot hit the non-forward tagging device and are thus completely inclusive. Due to this, a direct application of (4.1) is justified as a reasonable approximation and the neglect of identity of the photons is expected to be not very influential. The cross-section with account of leptonic initial-state LLA corrections will be:

$$\frac{d^3\sigma_{(i)}}{d \cos \theta'_e dE'_e dE_\gamma^{\text{vis}}} = \frac{d^3\sigma_{\text{brem}}}{d \cos \theta'_e dE'_e dE_\gamma^{\text{vis}}} + \frac{d^3\sigma_{(i)}^{\text{ini}}}{d \cos \theta'_e dE'_e dE_\gamma^{\text{vis}}}, \quad (4.7)$$

with

$$\begin{aligned} \frac{d^3\sigma_{(i)}^{\text{ini}}}{d \cos \theta'_e dE'_e dE_\gamma^{\text{vis}}} &= \int_{\Delta\Omega_\gamma} d \cos \theta_\gamma d\varphi_\gamma \int_0^1 dz \rho(z) \left\{ \frac{d^5\sigma_{\text{brem}}}{d \cos \theta'_e dE'_e d \cos \theta_\gamma d\varphi_\gamma dE_\gamma} \Big|_{E_e \rightarrow zE_e} \Theta_z \right. \\ &\quad \left. - \frac{d^5\sigma_{\text{brem}}}{d \cos \theta'_e dE'_e d \cos \theta_\gamma d\varphi_\gamma dE_\gamma} \right\}. \end{aligned} \quad (4.8)$$

4.2 Case (ii): Forward Tagging Device

Case (ii) is realized in the HERA detectors. Here, the situation is much more involved. One could make the assumption that nearly every one of the initial state (LLA) photons is emitted collinearly, carries energy $(1 - z)E_e$ and will hit the forward tagging device if its geometrical size is big enough. A simple estimate based on an analysis of the

denominator of the initial electron propagator after emission of the photon shows that the tagging device must have a geometric size fulfilling the condition

$$\Delta\theta_\gamma \gg \frac{m_e}{E_e} \quad (4.9)$$

in order to collect most of these photons. For an opening angle $\Delta\theta_\gamma = 0.5$ mrad and $E_e = 25$ GeV this condition is fulfilled but not to such an extent that numerical estimates of the LLA corrections would be sufficiently well. In fact, the tagging device induces a cut on the photon angle and leads to an additional logarithmic dependence of the cross-section on it⁶.

We have to distinguish several contributions. If both photons hit the tagging device, i.e.:

$$0 \leq \theta_\gamma \leq \Delta\theta_\gamma, \quad (4.10)$$

the visible photon energy has to be defined as the sum

$$E_\gamma^{\text{vis,(iia)}} = (1 - z)E_e + E_\gamma. \quad (4.11)$$

Next, if the photon of the lowest-order scattering process does not hit the photon tagger, i.e.:

$$\theta_\gamma > \Delta\theta_\gamma, \quad (4.12)$$

only the collinear LLA photon contributes to

$$E_\gamma^{\text{vis,(iib)}} = (1 - z)E_e. \quad (4.13)$$

Finally, it may happen that the LLA photon does not hit the tagger, but the lowest-order photon does:

$$0 \leq \theta_\gamma \leq \Delta\theta_\gamma, \quad (4.14)$$

and the visible photon energy is

$$E_\gamma^{\text{vis,(iic)}} = E_\gamma. \quad (4.15)$$

All three cases contribute to the cross-section and have to be summed up with the lowest-order cross-section:

$$\begin{aligned} \frac{d^3\sigma_{(ii)}}{d \cos \theta'_e dE'_e dE_\gamma^{\text{vis}}} &= \frac{d^3\sigma_{\text{brem}}}{d \cos \theta'_e dE'_e dE_\gamma^{\text{vis}}} + \frac{d^3\sigma_{(iia)}^{\text{ini}}}{d \cos \theta'_e dE'_e dE_\gamma^{\text{vis}}} \\ &+ \frac{d^3\sigma_{(iib)}^{\text{ini}}}{d \cos \theta'_e dE'_e dE_\gamma^{\text{vis}}} + \frac{d^3\sigma_{(iic)}^{\text{ini}}}{d \cos \theta'_e dE'_e dE_\gamma^{\text{vis}}}. \end{aligned} \quad (4.16)$$

⁶ LLA corrections with photon tagging have been discussed in [3], where a bremsstrahlung cross-section, reduced by tagged events, was estimated. The aim was to reduce the radiative corrections from hard photon emission. Our modifications of the density function by photon cuts are quite similar to the treatment in [3].

We now have to extract E_γ^{vis} from (4.1). This will be done in the next three subsections with use of identity δ -function integrations:

$$1 \equiv \int dE_\gamma^{\text{vis}} \delta \left[E_\gamma^{\text{vis}} - (1-z)E_e - E_\gamma \right], \quad (4.17)$$

$$1 \equiv \int dE_\gamma^{\text{vis}} \delta \left[E_\gamma^{\text{vis}} - (1-z)E_e \right], \quad (4.18)$$

$$1 \equiv \int dE_\gamma^{\text{vis}} \delta \left[E_\gamma^{\text{vis}} - E_\gamma \right]. \quad (4.19)$$

The three cases will be treated separately.

4.2.1 Case (iia): Both photons hit the forward tagging device

When two photons hit the forward tagging device, the cross-section gets:

$$\begin{aligned} \frac{d^3\sigma_{(iia)}^{\text{ini}}}{d \cos \theta'_e dE'_e dE_\gamma^{\text{vis}}} &= \int_0^1 dz \rho_a(z) \\ &\times \left\{ \frac{d^2\sigma_{\text{QED}}}{d \cos \theta'_e dE'_e} \Big|_{E_e \rightarrow zE_e} \Theta_z - \frac{d^2\sigma_{\text{QED}}}{d \cos \theta'_e dE'_e} \right\} \delta \left[E_\gamma^{\text{vis}} - (1-z)E_e - E_\gamma \right] \\ &= \int_{1-\frac{\Delta\theta_\gamma^2}{2}}^1 d \cos \theta_\gamma \int_0^{2\pi} d\varphi_\gamma \int_0^1 dz \rho_a(z) \\ &\times \left\{ \int_0^{\hat{E}_\gamma^{\text{max}}} dE_\gamma \left[\frac{d^5\sigma_{\text{brem}}}{d \cos \theta'_e dE'_e d \cos \theta_\gamma d\varphi_\gamma dE_\gamma} \Theta(E_\gamma - \bar{E}_\gamma) \right. \right. \\ &+ \left. \frac{1}{4\pi} \frac{d^2\sigma_{\text{VR}}}{d \cos \theta'_e dE'_e} \delta(E_\gamma) \right] \Big|_{E_e \rightarrow zE_e} \Theta_z \\ &- \int_0^{E_\gamma^{\text{max}}} dE_\gamma \left[\frac{d^5\sigma_{\text{brem}}}{d \cos \theta'_e dE'_e d \cos \theta_\gamma d\varphi_\gamma dE_\gamma} \Theta(E_\gamma - \bar{E}_\gamma) \right. \\ &+ \left. \left. \frac{1}{4\pi} \frac{d^2\sigma_{\text{VR}}}{d \cos \theta'_e dE'_e} \delta(E_\gamma) \right] \right\} \delta \left[E_\gamma^{\text{vis}} - (1-z)E_e - E_\gamma \right]. \quad (4.20) \end{aligned}$$

As mentioned, the density $\rho_a(z)$ will deviate from the inclusive density (4.2) due to the angular cut:

$$\rho_a(z) = \frac{\alpha}{2\pi} \frac{1+z^2}{1-z} \left(\ln \frac{m^2 + E_e^2 \Delta\theta_\gamma^2}{m^2} - 1 \right). \quad (4.21)$$

After performing the integral over z and some trivial re-orderings, we arrive at

$$\begin{aligned} \frac{d^3\sigma_{(iia)}^{\text{ini}}}{d \cos \theta'_e dE'_e dE_\gamma^{\text{vis}}} &= \int_{1-\frac{\Delta\theta_\gamma^2}{2}}^1 d \cos \theta_\gamma \int_0^{2\pi} d \cos \varphi_\gamma \int_{\max\{\bar{E}_\gamma, E_\gamma^{\text{min}}\}}^{\min\{E_\gamma^{\text{vis}}, E_\gamma^{\text{max}}\}} dE_\gamma \\ &\times \frac{\rho_a(z)}{E_e} \Big|_{z=1-\frac{E_\gamma^{\text{vis}}-E_\gamma}{E_e}} \left[\frac{d^5\sigma_{\text{brem}}}{d \cos \theta'_e dE'_e d \cos \theta_\gamma d\varphi_\gamma dE_\gamma} \Big|_{E_e \rightarrow zE_e} \Theta_z \right. \\ &- \left. \frac{d^5\sigma_{\text{brem}}}{d \cos \theta'_e dE'_e d \cos \theta_\gamma d\varphi_\gamma dE_\gamma} \right] \end{aligned}$$

$$\begin{aligned}
& + \frac{\Delta\Omega_\gamma^{(iia)}}{4\pi} \frac{\rho_a(z)}{E_e} \Big|_{z_{\min}=1-\frac{E_\gamma^{\text{vis}}}{E_e}} \left[\frac{d^2\sigma_{\text{VR}}}{d\cos\theta'_e dE'_e} \Big|_{E_e \rightarrow z_{\min}E_e} \Theta_{z_{\min}} \right. \\
& \left. - \frac{d^2\sigma_{\text{VR}}}{d\cos\theta'_e dE'_e} \right] \Theta(z_{\min} - z_0). \tag{4.22}
\end{aligned}$$

Everything is straightforward in the above derivation. The only delicate point is the determination of the boundaries for the integration over E_γ , and, related to this, the allowed range for E_γ^{vis} . This will be explained in some detail now with use of Figure 4. The integration over E_γ proceeds along one of the dotted straight lines with defining equation (4.17):

$$E_\gamma = (E_\gamma^{\text{vis}} - E_e) + z E_e. \tag{4.23}$$

The absolute maximum of E_γ^{vis} is reached for $z = 1$, and the absolute minimum for:

$$z_{\min} = 1 - \frac{E_\gamma^{\text{vis}}}{E_e}, \tag{4.24}$$

where E_γ vanishes. For the hard photon integral in (4.22) this minimum has to be replaced by \bar{E}_γ as discussed above. The discussion of limits would be finished here if there wouldn't be the scaled kinematical upper limit for E_γ , $\bar{E}_\gamma^{\text{max}}$, which also has to be respected. This limit depends on several variables: $z, E_e, E_p, E'_e, \theta'_e, \varphi_\gamma, \theta_\gamma$.

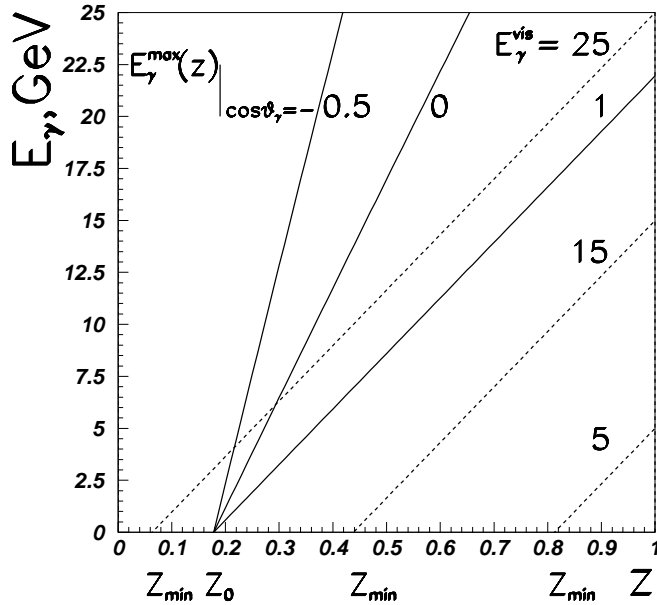


Figure 4: *The physical region (z, E_γ) for Case (iia): both photons hit the forward tagging device*

From (2.20) one may see that the minimum value of E_γ^{\max} , which is zero, is independent of the actual values of the photonic angular variables. It depends, besides on E_p , on zE_e and external variables E'_e, θ'_e and is reached for fixed E'_e, θ'_e at some value z_0 which may be easily derived from (A.4) (with neglected terms of order $\mathcal{O}(m^2)$):

$$z_0 = z_0(E_e, E_p, E'_e, \theta'_e) = \frac{\bar{M}^2 - (p_1 - k_2)^2}{2k_1(p_1 - k_2)}. \quad (4.25)$$

As is visualized in Figure 4, z_0 may be bigger or smaller than z_{\min} in dependence on E_γ^{vis} . If z_0 is smaller than z_{\min} , it is of no influence on the integration region and the lower integration boundary is \bar{E}_γ . In the other case, one has to study in detail where the necessary condition $E_\gamma^{\max} > E_\gamma^{\text{vis}}$ is fulfilled. Some value z_1 , corresponding to some value E_γ^{\min} may be found where this begins to be fulfilled and the lower integration boundary becomes E_γ^{\min} :

$$E_\gamma^{\min} = E_\gamma^{\max}(z_1 E_e, E_p; E'_e, \varphi_\gamma, \theta_\gamma, \theta'_e) = E_\gamma^{\text{vis}} - (1 - z_1)E_e. \quad (4.26)$$

Therefore, $d^2\sigma_{\text{VR}}$ will not contribute to (4.22).

We further have to study the fan of curves defining the value of E_γ^{\max} , starting from z_0 and depending on the parameters $\theta_\gamma, \varphi_\gamma$ as a function of z at fixed E'_e, θ'_e . Figure 4 shows that, for HERA kinematics, the curves are nearly straight lines. If their curvature is strong enough, they may cross the straight dotted integration path from above, in principle independent of the relation between z_0 and z_{\min} . If this happens the upper integration limit in (4.22) is not E_γ^{vis} but \bar{E}_γ^{\max} . The figure suggests that for the case of a forward tagging device (with $\cos\theta_\gamma \approx 1$) the relevant solid curve is nearly parallel to the dotted line. Then, for reasonable choices of E_γ^{vis} no problems should occur from details of the kinematics.

To conclude the discussion, one has to integrate the scaled cross-section over all values of E_γ on one of the dotted lines which are located below the envelop of the fan of curves $E_\gamma^{\max}(z)$. The unscaled cross-sections are integrated from \bar{E}_γ to E_γ^{vis} . In applications, we restrict ourselves to kinematics with $z_0 < z_{\min}$ and $E_\gamma^{\max} > E_\gamma^{\text{vis}}$. The FORTRAN program stops if $z_{\min} < z_0$.

4.2.2 Case (iib): The LLA photon hits the forward tagging device

If only the collinear initial-state LLA photon hits the forward tagging device, the cross-section becomes:

$$\begin{aligned} \frac{d^3\sigma_{(iib)}^{\text{ini}}}{d\cos\theta'_e dE'_e dE_\gamma^{\text{vis}}} &= \int_0^1 dz \rho_b(z) \\ &\times \left\{ \frac{d^2\sigma_{\text{QED}}}{d\cos\theta'_e dE'_e} \Big|_{E_e \rightarrow zE_e} \Theta_z - \frac{d^2\sigma_{\text{QED}}}{d\cos\theta'_e dE'_e} \right\} \delta [E_\gamma^{\text{vis}} - (1 - z)E_e] \\ &= \int_{-1}^{1 - \frac{\Delta\theta_\gamma^2}{2}} d\cos\theta_\gamma \int_0^{2\pi} d\varphi_\gamma \int_0^1 dz \rho_b(z) \\ &\times \left\{ \int_0^{\hat{E}_\gamma} dE_\gamma \left[\frac{d^5\sigma_{\text{brem}}}{d\cos\theta'_e dE'_e d\cos\theta_\gamma d\varphi_\gamma dE_\gamma} \Theta(E_\gamma - \bar{E}_\gamma) \right. \right. \end{aligned}$$

$$\begin{aligned}
& + \frac{1}{4\pi} \frac{d^2 \sigma_{\text{VR}}}{d \cos \theta'_e dE'_e} \delta(E_\gamma) \Big|_{E_e \rightarrow z E_e} \Theta_z \\
& - \int_0^{E_\gamma^{\text{max}}} dE_\gamma \left[\frac{d^5 \sigma_{\text{brem}}}{d \cos \theta'_e dE'_e d \cos \theta_\gamma d\varphi_\gamma dE_\gamma} \Theta(E_\gamma - \bar{E}_\gamma) \right. \\
& \left. + \frac{1}{4\pi} \frac{d^2 \sigma_{\text{VR}}}{d \cos \theta'_e dE'_e} \delta(E_\gamma) \right] \Big\} \delta \left[E_\gamma^{\text{vis}} - (1-z)E_e \right]. \quad (4.27)
\end{aligned}$$

The density function for the LLA correction is the same as that for Case (ia):

$$\rho_b(z) = \rho_a(z). \quad (4.28)$$

The subsequent formal steps differ from Case (ia) since E_γ is not involved in the δ -function. The limits of variation of E_γ are affected only by scaling:

$$\begin{aligned}
\frac{d^3 \sigma_{(iib)}^{\text{ini}}}{d \cos \theta'_e dE'_e dE_\gamma^{\text{vis}}} &= \frac{\rho_a(z)}{E_e} \Big|_{z_{\text{min}}=1-\frac{E_\gamma^{\text{vis}}}{E_e}} \left\{ \int_{-1}^{1-\frac{\Delta\theta_\gamma^2}{2}} d \cos \theta_\gamma \int_0^{2\pi} d \cos \varphi_\gamma \right. \\
& \times \int_{\bar{E}_\gamma}^{\min\{E_\gamma^{\text{res}}, E_\gamma^{\text{max}}\}} dE_\gamma \left[\frac{d^5 \sigma_{\text{brem}}}{d \cos \theta'_e dE'_e d \cos \theta_\gamma d\varphi_\gamma dE_\gamma} \Big|_{E_e \rightarrow z_{\text{min}} E_e} \Theta_{z_{\text{min}}} \right. \\
& \quad \left. - \frac{d^5 \sigma_{\text{brem}}}{d \cos \theta'_e dE'_e d \cos \theta_\gamma d\varphi_\gamma dE_\gamma} \right] \\
& \left. + \frac{\Delta\Omega_\gamma^{(iib)}}{4\pi} \left[\frac{d^2 \sigma_{\text{VR}}}{d \cos \theta'_e dE'_e} \Big|_{E_e \rightarrow z_{\text{min}} E_e} \Theta_{z_{\text{min}}} - \frac{d^2 \sigma_{\text{VR}}}{d \cos \theta'_e dE'_e} \right] \right\}. \quad (4.29)
\end{aligned}$$

The integration boundaries may be inspected in Figure 5. One should notice that the upper integration limit is again different for the scaled and the unscaled cross-section integration. In (4.29), the unscaled integration limits are used, however. In the figure, they define the solid straight line ranging from the point $(z, E_\gamma) = (1, \bar{E}_\gamma)$ upwards until it meets the actual value of E_γ^{max} ; the latter depends on the kinematics. The scaled limits are dependent on z and define a dotted straight line at fixed z_{min} . These limits are automatically respected by means of the factor $\Theta_{z_{\text{min}}}$ in (4.29).

Further, we introduced a new variable, E_γ^{res} , in the definition of the upper integration bound. If somebody wants to impose a general cut on the maximum allowed photon energy, it has to be done here and only here.

4.2.3 Case (iic): The LLA photon does not hit the forward tagging device

This case is very similar to Case (i). The correction may be read off from (4.8) with a modified density ρ_c due to the cut on the angular integration for the LLA photon and with performing the angular integration for the Born photon as in Case (ia):

$$\begin{aligned}
\frac{d^3 \sigma_{(iic)}^{\text{ini}}}{d \cos \theta'_e dE'_e dE_\gamma^{\text{vis}}} &= \int_{1-\frac{\Delta\theta_\gamma^2}{2}}^1 d \cos \theta_\gamma \int_0^{2\pi} d\varphi_\gamma \int_0^1 dz \rho_c(z) \\
& \left\{ \frac{d^5 \sigma_{\text{brem}}}{d \cos \theta'_e dE'_e d \cos \theta_\gamma d\varphi_\gamma dE_\gamma} \Big|_{E_e \rightarrow z E_e} \Theta_z \right.
\end{aligned}$$

$$\left. - \frac{d^5 \sigma_{\text{brem}}}{d \cos \theta'_e dE'_e d \cos \theta_\gamma d\varphi_\gamma dE_\gamma} \right\}, \quad (4.30)$$

with

$$\rho_c(z) = \frac{\alpha}{2\pi} \frac{1+z^2}{1-z} \ln \frac{Q^2}{m^2 + E_e^2 \Delta\theta_\gamma^2}. \quad (4.31)$$

5 Numerical Results and Discussion

Numerical results are shown for the H1 forward tagging device, which is approximated here by a circle located symmetrically around the beam axis with $\Delta\theta_\gamma = 0.5$ mrad. The lowest-order cross-section has been shown in Section 2. The estimated radiative corrections δ ,

$$\delta = \frac{d^3 \sigma^{\text{ini}}/dx dy dE_\gamma^{\text{vis}}}{d^3 \sigma_{\text{brem}}/dx dy dE_\gamma^{\text{vis}}} \times 100\%, \quad (5.32)$$

are shown in Figures 6 and 7. The $d^3 \sigma^{\text{brem}}$ is defined in (2.34) and $d^3 \sigma^{\text{ini}}$ in (4.7) or (4.16).

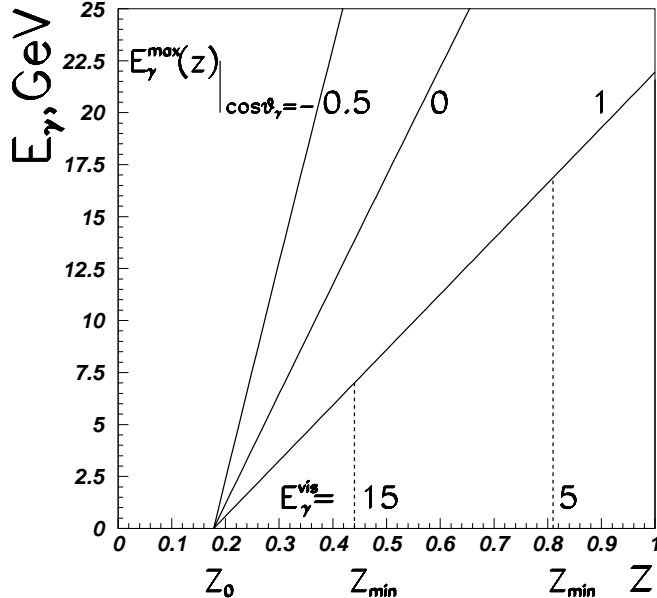


Figure 5: *The physical region (z, E_γ) for Case (iib): only the LLA photon hit the forward tagging device*

For the figures, we consider Case (ii) (forward tagging) and assume $E_\gamma^{\text{vis}} = 5$ GeV and $E_\gamma^{\text{vis}} = 10$ GeV. The maximal allowed photon energy is assumed not to be restricted;

this corresponds to no photon observation outside the tagging device. As was mentioned already in the discussion of the Born cross-section, there is a minimal value y_c of y which depends on the kinematics $(x, y, E_\gamma^{\text{vis}})$. Otherwise, the resulting corrections are similar to those known from the inclusive measurements. The Born cross-section dies out for $x > 10^{-4}$, thus limiting the Q^2 values at HERA to be not bigger than several GeV^2 . For nearly all this kinematical range, the corrections stay well in between about $\pm 20\%$, mostly even within 0 and 10%. Larger, negative QED corrections arise in the soft photon corner (at small y) and large positive ones for hard radiation at high y . The biggest, negative corrections are obtained at larger values of x where the Born rates go down rapidly. The soft photon corrections are weakened by higher-order contributions. These may be taken into account by performing soft photon exponentiation. An approximation could be to do this for either the lowest-order bremsstrahlung cross-section or the LLA density function separately. An explicit higher-order calculation is needed for a sufficiently correct answer. The numbers in the figures were produced without soft photon exponentiation.

In this article, we studied deep inelastic cross-sections at HERA energies with photon tagging. The lowest-order radiative process is calculated in ultra-relativistic approximation with no additional restricting assumptions. The next-order corrections have been estimated with a leading-logarithmic approximation neglecting the interferences between diagrams with different topology concerning the two photons. The resulting error is expected to be of next-to-leading order and could be non-negligible for a forward tagging device. Our calculations are performed strictly in order $\mathcal{O}(\alpha)$. For soft photon emission, we know to overestimate the large, negative corrections. An exponentiation of soft photon corrections is recommended here if one wants to improve the numerical results. Again, problems due to interference effects remain unsolved so far. For a forward tagger, the problem is not completely inclusive. Logarithmic corrections due to the finite size of the tagger are taken into account.

Since the calculated corrections are not too big compared to the typical size of photonic corrections in deep inelastic scattering one may expect that they represent a quite good approximation of a complete calculation of the order $\mathcal{O}(\alpha)$ photonic corrections.

Acknowledgements

We are grateful to J. Feltesse for drawing our interest to this problem. We are indebted to A. Arbuzov, A. Glazov, and M. Klein for fruitful discussions, to S. Jadach for directing our attention to reference [3], and to H. Anlauf, L. Favart, F. Jegerlehner and M. Klein for a careful reading of the manuscript and comments.

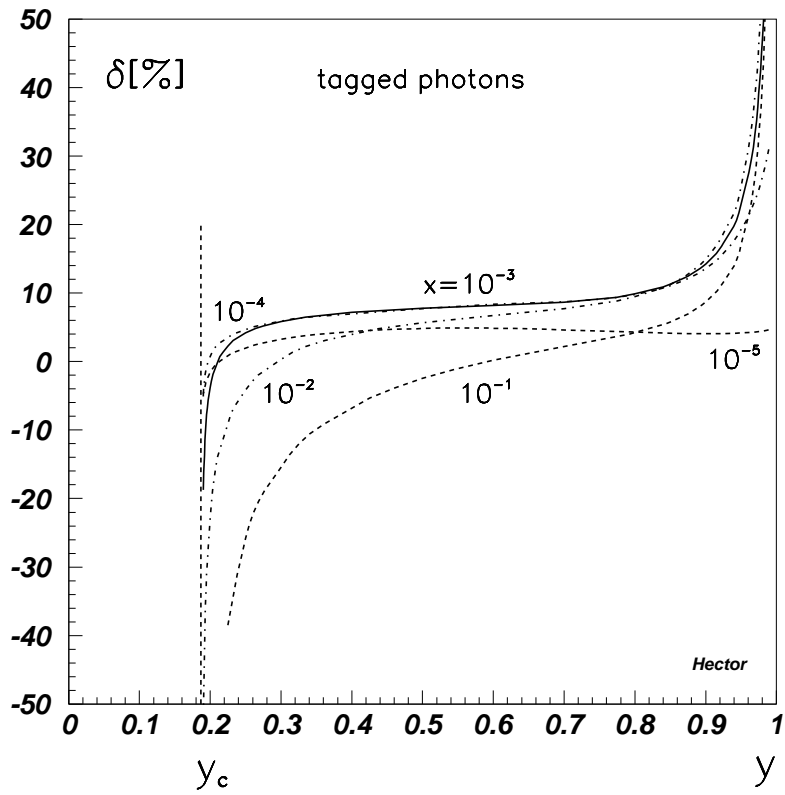


Figure 6: Photonic correction $\delta = d^3\sigma^{\text{ini}}/d^3\sigma_{\text{brem}} \times 100\%$ for $E_\gamma^{\text{vis}} = 5 \text{ GeV}$ and $\Delta\theta_\gamma = 0.5 \text{ mrad}$ for a forward tagging device

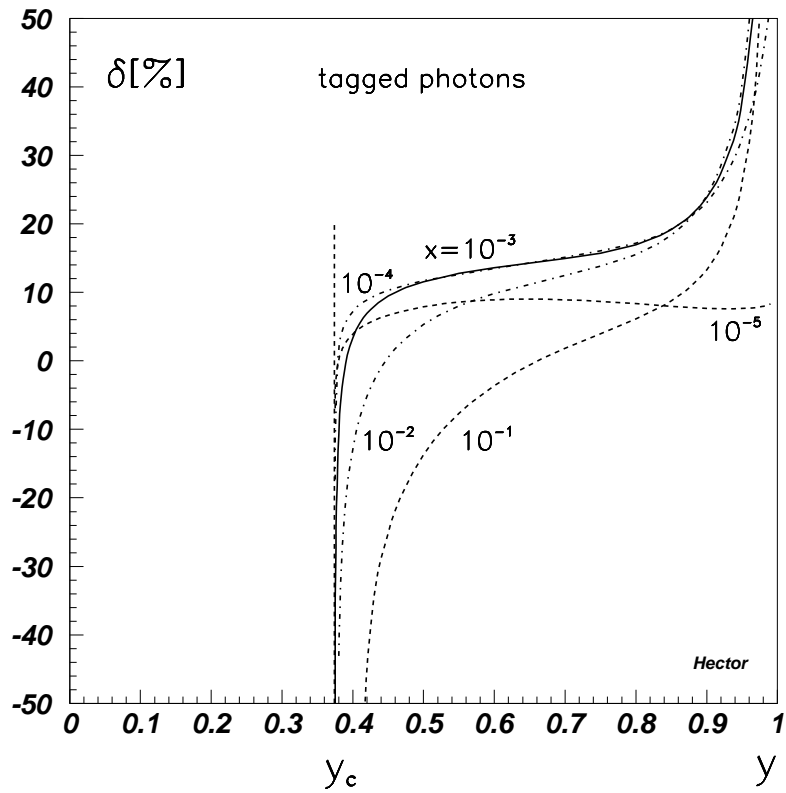


Figure 7: *The same as figure 6 but with $E_\gamma^{\text{vis}} = 10 \text{ GeV}$*

A Kinematics and Phase Space

The angular variables $\theta'_e, \theta_\gamma, \varphi_\gamma$ are unrestricted. The lower limits of E'_e and E_γ are m and zero, respectively.

The upper limits of the two energies depend on the order of integration. We calculate the cross-sections in terms of the electron variables E'_e, θ'_e . Therefore, we call them *external* variables and may derive the corresponding boundary from the condition

$$\begin{aligned} W^2 &= (k_1 + p_1 - k_2)^2 \\ &= (E_e + E_p - E'_e)^2 - (p'_e)^2 - (p_e - p_p)^2 + 2p'_e(p_e - p_p)\cos\theta'_e \\ &\geq \bar{M}^2. \end{aligned} \quad (\text{A.1})$$

Solving this inequality for E'_e yields (2.16).

The two-dimensional region of variation of $\cos\theta'_e$ and E'_e is shown in Figure 8. Photonic variables are considered to be varying at fixed values of electron variables and will be called *internal* variables. The limit for E_γ follows from a condition which relates k_2 and k properly. It is:

$$M_h^2 = (p_1 + k_1 - k_2 - k)^2 \geq \bar{M}^2. \quad (\text{A.2})$$

In terms of natural variables:

$$\begin{aligned} M_h^2 &= W^2 \\ &\quad - 2E_\gamma \left\{ [p'_e \cos\theta'_e - (p_e - p_p)] \cos\theta_\gamma + p'_e \sin\theta'_e \sin\theta_\gamma \cos\varphi_\gamma - E'_e + E_e + E_p \right\}, \end{aligned} \quad (\text{A.3})$$

from which we get

$$E_\gamma^{\max} = \frac{W^2 - \bar{M}^2}{2[E_e + E_p - E'_e + (p'_e \cos\theta'_e - [p_e - p_p]) \cos\theta_\gamma + p'_e \sin\theta'_e \sin\theta_\gamma \cos\varphi_\gamma]}, \quad (\text{A.4})$$

which in fact is (2.20).

In the ultra-relativistic approximation in m , (2.20) reduces for $\theta_\gamma = 0$ to

$$E_\gamma^{\max} = \frac{2E_e E_p + (M^2 - \bar{M}^2)/2 - E_e E'_e (1 - \cos\theta'_e) - E_p E'_e (1 + \cos\theta'_e)}{2E_p - E'_e (1 - \cos\theta'_e)}, \quad (\text{A.5})$$

and for $\theta_\gamma = \pi$ to

$$E_\gamma^{\max} = \frac{2E_e E_p + (M^2 - \bar{M}^2)/2 - E_e E'_e (1 - \cos\theta'_e) - E_p E'_e (1 + \cos\theta'_e)}{2E_e - E'_e (1 + \cos\theta'_e)}, \quad (\text{A.6})$$

These limiting cases are of use for an understanding of the plots of kinematical boundaries of variation of the *internal* variables $\cos\theta_\gamma, \varphi_\gamma, E_\gamma$ which are shown in Figure 9.

Next we have to discuss the phase space parameterization. We aim at a check on the correctness of the kinematical boundaries since the angular bounds have not been explicitly derived.

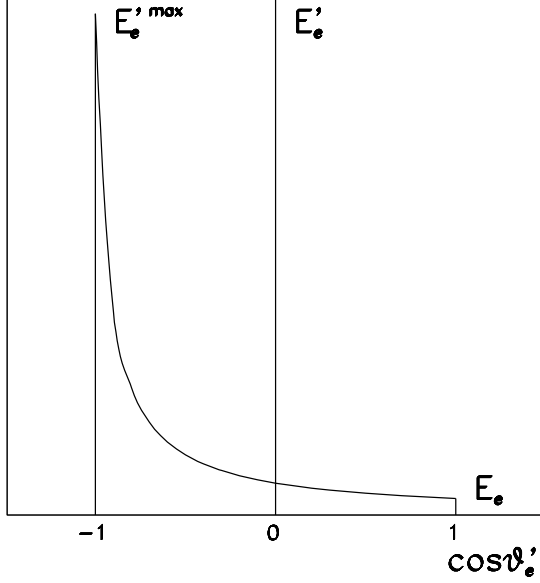


Figure 8: *Kinematical boundaries for $\cos \theta'_e$ and E'_e*

In Eq. (I.3.9) we made use of a parameterization of the phase space in terms of the invariants y_l, Q_l^2, y_h, Q_h^2 , together with one additional variable z_2 (or z_1):

$$d\Gamma = \frac{\pi^2 S}{4} dy_l dQ_l^2 dy_h dQ_h^2 \frac{dz_{1(2)}}{\pi \sqrt{R_z}}. \quad (\text{A.7})$$

From explicit expressions for y_l and Q_l^2 in terms of natural variables it is easy to derive the Jacobean

$$dy_l dQ_l^2 = 2p'_e dE'_e d\cos \theta'_e. \quad (\text{A.8})$$

From (A.7) and (A.8) we get the doubly-differential phase space in terms of $\cos \theta'_e, E'_e$ from a three-fold integration over invariants with the aid of Eqs. (I.D.2), (I.C.2), (I.C.3):

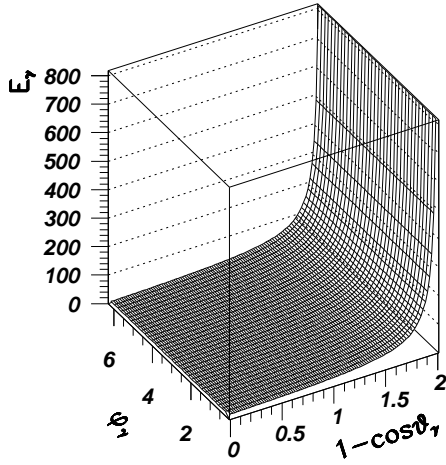
$$\frac{d\Gamma}{p'_e dE'_e d\cos \theta'_e} = \frac{\pi^2 S}{2} \int_{\bar{M}^2}^{W^2} dM_h^2 \int_{Q_{h,\min}^2}^{Q_{h,\max}^2} dQ_h^2 \int_{z_{\min}}^{z_{\max}} \frac{dz_{1(2)}}{\pi \sqrt{R_z}} = \frac{\pi^2 (W^2 - M^2)^2}{4W^2}, \quad (\text{A.9})$$

where we also used (I.3.7):

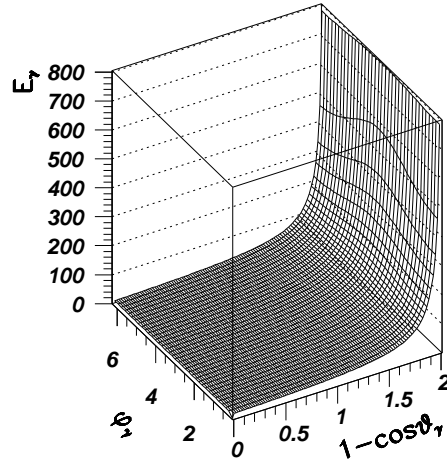
$$dy_h dQ_h^2 = \frac{1}{S} dM_h^2 dQ_h^2. \quad (\text{A.10})$$

On the other hand, the phase space (A.9) in terms of natural variables was given in (2.23):

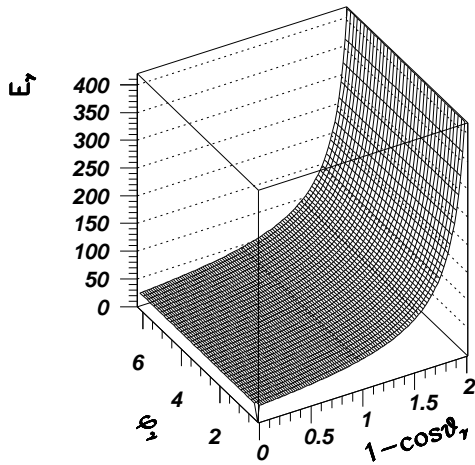
$$\frac{d\Gamma}{p'_e dE'_e d\cos \theta'_e} = \frac{\pi}{2} \int_0^{2\pi} d\varphi_\gamma \int_{-1}^{+1} d\cos \theta_\gamma \int_0^{E_\gamma^{\max}} E_\gamma dE_\gamma. \quad (\text{A.11})$$



a) $\cos\theta'_e=1, E'_e=15$



b) $\cos\theta'_e=0, E'_e=25$



c) $\cos\theta'_e=-1, E'_e=400$

Figure 9: *Kinematical boundaries for $\cos\theta_\gamma, \varphi_\gamma, E_\gamma$ at given values of E'_e and $\cos\theta'_e$*

We checked numerically that the phase space (A.9) agrees within computer precision (14 digits) with the new expression (2.23) if one uses in (A.9) the W^2 introduced in (A.1).

Finally, we have to collect the integrals for the calculation of $\delta_{\text{hard}}^{\text{IR}}$:

$$[A] = \frac{1}{\pi} \int_{\epsilon}^{\bar{E}_\gamma} dE_\gamma E_\gamma \int_{-1}^1 d \cos \theta_\gamma \int_0^{2\pi} d\varphi_\gamma A. \quad (\text{A.12})$$

For sufficiently small \bar{E}_γ there is no dependence of the angular integration limits on E_γ . In this case, the integrations are straightforward and the results are very simple:

$$\left[\frac{m^2}{z_1^2} \right] = \left[\frac{m^2}{z_2^2} \right] = \ln \frac{\bar{E}_\gamma}{\epsilon}, \quad (\text{A.13})$$

$$\left[\frac{1}{z_1 z_2} \right] = 2L_m \ln \frac{\bar{E}_\gamma}{\epsilon}, \quad (\text{A.14})$$

and L_m is defined in (3.17). The above two integrals are the equivalent of the tables of integrals in appendix (I.D.3) for the present calculations.

References

- [1] A. Akhundov, D. Bardin, L. Kalinovskaya and T. Riemann, *Fortschritte d. Physik* **44** (1996) 373-482.
- [2] A. Arbuzov, D. Bardin, J. Blümlein, L. Kalinovskaya and T. Riemann, Fortran program HECTOR, *Comp. Phys. Commun.* **94** (1996) 128-184.
- [3] S. Jadach, M. Jezabek and W. Placzek, *Phys. Letters* **B248** (1990) 417.